I&EC research
Industrial & Engineering Chemistry Research
pubs.acs.org/IECR

Article

Double-Eccentric Design for the Vortex Finder of a Cyclone Separator

Yuge Yao, Zhong Huang,* Tuo Zhou, Jinjing Li, Liang Cheng, Man Zhang, Hairui Yang, and Junfu Lyu

Cite This: *Ind. Eng. Chem. Res.* 2022, 61, 14927−14939

Read Online

ACCESS | Metrics & More | Article Recommendations | Supporting Information

ABSTRACT: In the present study, a double-eccentric design for the vortex finder of a cyclone separator was proposed to enhance the cyclone performance. Using the numerical approaches, the flow field inside the cyclone was simulated and the cyclone performance was evaluated. The orthogonal method was adopted to obtain the optimal structure of the double-eccentric vortex finder. The range analysis of the five key geometric factors in the double-eccentric design was also conducted. It was found that cyclone performance is more sensitive to the eccentricity of the vortex finder than the other factors. The best eccentric angle of the inlet of the vortex finder is 270°, which markedly improves the separation efficiency and slightly increases the pressure drop. The simulated flow field depicted that the double-eccentric vortex finder results in the strongest swirling flow in the middle and lower parts of the cyclone compared with the vortex finders of the original, non-eccentric, and single-eccentric designs. The results also reflected that off-centering the vortex finder has the most significant impact on the flow patterns. Moreover, an industrial test was carried out in a circulating fluidized bed boiler for this novel vortex finder. The fly ash of the double-eccentric vortex finder becomes finer and contains less carbon content than that of the original one, which indicates that the double-eccentric vortex finder successfully enhances the separation performance.

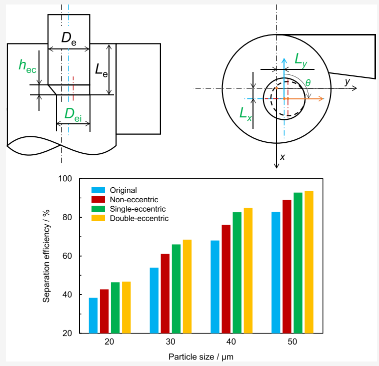

1. INTRODUCTION

The cyclone separator has been widely applied in various gas-particle separation processes due to its simple structure and good separation performance.[1,2] A typical cyclone separator consists of an inlet duct, cylinder body, cone tip, and vortex finder. The structure of the cyclone plays a critical role in the inside flow pattern and, therefore, has a great impact on the performance of the cyclone. The cyclone performance can be effectively improved by adjusting the structural parameters.

As the upper outlet of the cyclone, the vortex finder is directly linked to the generation of the strong swirling flows. To develop the high-separation-efficiency cyclone, many studies on the structural optimization of the vortex finder have been carried out.

The diameter and length are the two basic geometry parameters of the most common cylindrical vortex finder. Iozia et al.[3] measured the gas velocity inside the cyclones of different designs and found that a thinner vortex finder results in higher maximum tangential velocity and also separation efficiency. Kim et al.[4] concluded that as the vortex finder diameter increases, the separation efficiency decreases while the pressure drop first decreases and then increases when the vortex finder diameter is close to the cylindrical body diameter. El-Batsh[5] computed the flow patterns in cyclones with different vortex finder diameters and lengths and provided the performance maps for the proper selection of the vortex finder. Elsayed et al.[6] reported that the vortex finder diameter has more significant effects on the cyclone performance compared to the vortex finder insertion depth. Zhang et al.[7] investigated the vortex finder structural parameters using numerical simulations and artificial neural networks. The tangential velocity index is more sensitive to the insertion depth than the vortex finder diameter. Razmi et al.[8] reported that lengthening the vortex finder can improve the separation efficiency. Hwang et al.[9] observed that the separation efficiency first increases and then decreases as the vortex finder becomes longer in a circulating fluidized bed (CFB) system. Tian et al.[10] attributed the change in the separation efficiency with the vortex finder length to the short-circuit flow when the vortex finder is located in the cylindrical section. When the vortex finder extended to the conical section, they attributed the change in the separation efficiency to the effects of the cylindrical−conical interface.

The shape of the vortex finder is also very important for cyclone performance. Lim et al.,[11] Ghodrat et al.,[12] and Wang et al.[13] studied the effects of the conical vortex on cyclone performance. The results indicated that a reversed conical vortex finder can improve the separation efficiency; however, a conical one can decrease the separation efficiency. A smaller

Received: June 10, 2022
Revised: September 16, 2022
Accepted: September 20, 2022
Published: September 27, 2022

vortex finder cone ratio results in higher separation efficiency and pressure drop. The effects of the conical part length on the cyclone performance are decided by the inlet solid concentration and are much less significant than those of the vortex finder diameter. Elsayed[14] designed a novel vortex finder with variable cross sections to minimize the pressure drop using the adjoint method. The simulated results also depicted that this novel vortex finder can increase the separation efficiency. Misiulia et al.[15] and de Souza et al.[16] focused on the part of the vortex finder outside the cylinder body. Their results showed that how the vortex finder extends from the cyclone top surface to the gas outlet surface can also influence the flow pattern and performance. Similarly, Luo et al.[17] tested three different connection modes between the vortex finder and the backpass in a CFB rig. The connection modes affect the cyclone performance due to the resistance coefficient.

Some researchers tried to optimize the vortex finder by changing the wall structure. Fu et al.[18] adopted the slotted vortex finder to increase the separation efficiency. Pei et al.[19] inserted blades at the bottom of the vortex finder, which significantly decrease the pressure drop and slightly increase the separation efficiency. Dziubak[20] adopted swirl vane blades in the vortex finder to reduce the escaped particles. Zhao et al.[21] discussed the wall thickness of the vortex finder and a thin-walled vortex finder was suggested. Vakamalla et al.[22] proposed the conical wall structure of the vortex finder. Wakizono et al.[23] attached a ring to the vortex finder to improve the separation efficiency. Li et al.[24] added a notch near the inlet of the vortex finder and found the best cut position while Dziubak[25] added bulges near the inlet of the vortex finder. Chen et al.[26] tested an edge-sloped vortex finder in a cold CFB rig and successfully increased the circulating flow rate. Chang et al.[27] set a built-in granular bed filter on the vortex finder to enhance the separation performance.

In addition to the above structural optimizations of the vortex finder, the design of the cyclone with an eccentric vortex finder has also been proposed and investigated. Muschelknautz et al.[28] applied the eccentric vortex finder in a pilot plant and successfully improve the separation performance. They attributed the increase in the separation efficiency to the prevention of the swirling flow detachment. The eccentric vortex finder is now very common in engineering practice.[29−32]

Some numerical studies were also conducted on the cyclone with an eccentric vortex finder. Brar et al.[33] evaluated the performance of more than 90 cyclones with eccentric vortex finders of various eccentricities and directions using the large eddy simulation and artificial neural network. They confirmed that appropriately off-centering the vortex finder provides a possible way to improve the separation efficiency. Parvaz et al.[34] performed a similar investigation on a gas−liquid cyclone and also reported that the eccentric vortex finder has a great effect on both the flow field and cyclone performance. Cocco et al.[35] simulated the flow fields in two cyclones with concentric and eccentric vortex finders and found that the eccentric vortex finder reduces the lower pressure region around the vortex finder which can diminish the secondary swirling flow and prevent more particles to escape.

Although many structural optimizations have been applied for better cyclone performance, there is still room for improvement, especially in the separation of fine particles.[36] Consequently, this study aims to make further improvements on the separation efficiency based on the eccentric vortex finder but avoids adding much complexity to the cyclone structure. Based on the above considerations, a novel vortex finder with a double-eccentric structure was proposed. A numerical simulation was conducted to estimate the performance of the cyclones with this novel vortex finder. Based on the orthogonal method, the optimal structure of the double-eccentric vortex finder was obtained. Finally, an industrial test for the above-mentioned optimal structure was implemented in a commercial CFB boiler.

2. OPTIMIZATION DESIGN FOR THE CYCLONE SEPARATOR

2.1. Double-Eccentric Design for the Vortex Finder.

The optimization design for the cyclone separator in this study is based on a conventional cylindrical−conical cyclone separator; see Figure 1. A contracted inlet duct is adopted to increase the gas velocity at the inlet of the cylinder body. The vortex finder is cylindrical in shape. The central axes of the vortex finder and cylinder body coincide, namely, the cross sections of the vortex finder and cylinder body are two concentric circles in the top view in Figure 1. The cylinder diameter (D) is 5.4 m. The other geometric dimensions of this cyclone separator are listed in Table S1 in the Supporting Information.

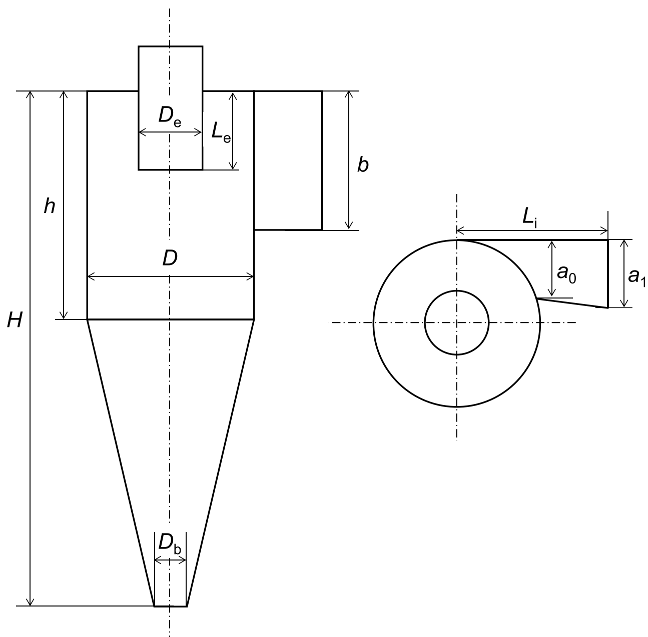

Figure 1. Schematic diagram of the conventional cyclone separator.

To improve the cyclone performance, the bottom of the vortex finder is modified to a reversed conical shape; see Figure 2. After entering the vortex finder, the gas flows first through the conical part where the flow area gradually expands, and then the cylindrical part. By changing the relative positions among the cylinder body and the two parts of the vortex finder, three designs are provided here. As shown in Figure 2a,b, for the non-eccentric and single-eccentric designs, the inlet and outlet of the vortex finder are concentric and the whole vortex finder has a central axis. While in the single-eccentric design the vortex finder and the cylinder body are eccentric and the vortex finder is on the lower right side of the cylinder body in the top view in Figure 2b. Based on the above two designs, the

https://doi.org/10.1021/acs.iecr.2c02054
Ind. Eng. Chem. Res. 2022, 61, 14927−14939

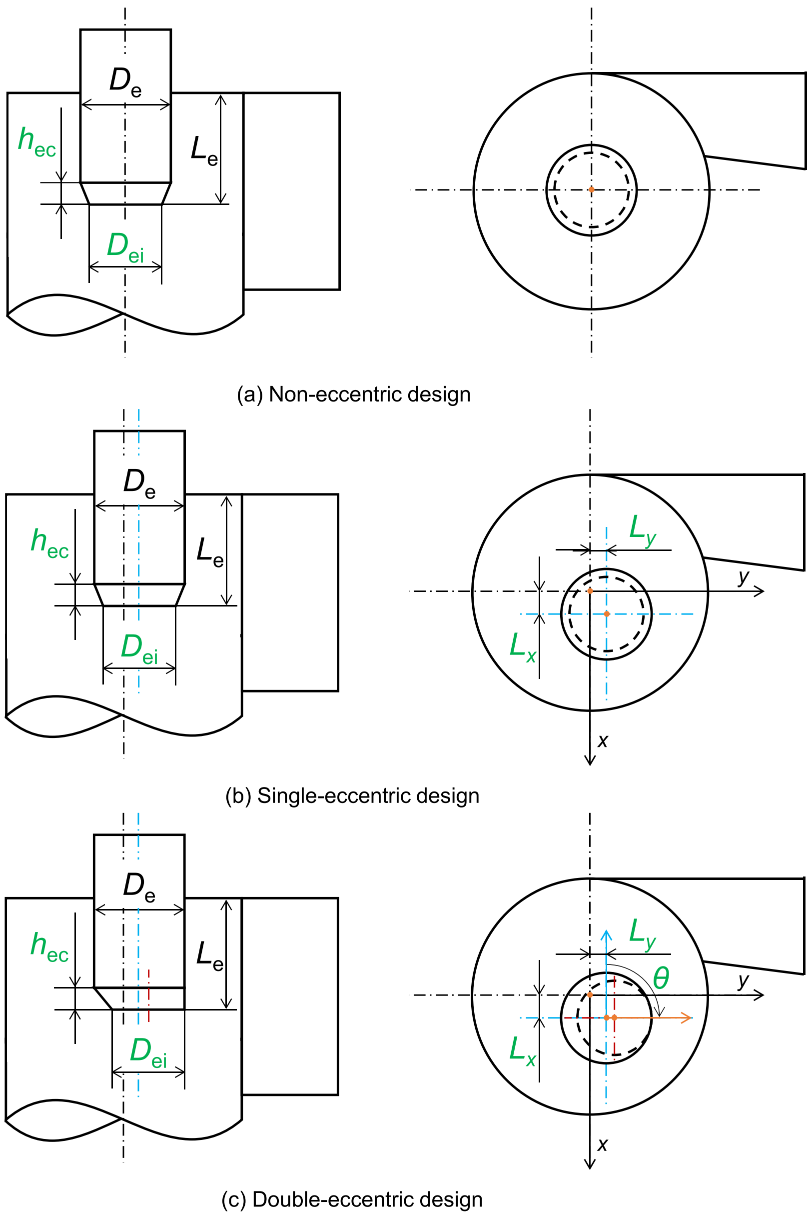

Figure 2. Schematic diagrams of the non-eccentric, single-eccentric, and double-eccentric designs for the vortex finder.

inlet of the vortex finder is inscribed in the outlet of the vortex finder in the double-eccentric design. As shown in Figure 2c, the double-eccentric design is constrained by five key geometric parameters including the inlet diameter of the vortex finder (D_{ei}), the height of the conical part (h_{ec}), the eccentricities of the vortex finder in the x direction (L_x) and y direction (L_y), and the eccentric angle of the inlet of the vortex finder (θ).

2.2. Orthogonal Method. The orthogonal method has been widely applied in studies that concern multiple factors.[37−39] In the present study, the orthogonal method was adopted to investigate the effects of the key parameters on the cyclone performance and find out the optimal structure of the double-eccentric design for the vortex finder. There are five factors in the orthogonal tests and each factor includes four levels listed in Table 1. Therefore, an $L_{16}(4^5)$ orthogonal table of the double-eccentric design was established and 16 structures of the vortex finder are summarized in Table 2.

Table 1. Factors and Levels of the Orthogonal Method

	factor				
level	D_{ei}/m	h_{ec}/m	L_x/m	L_y/m	θ/°
1	1.87	0.15	0	0	0
2	1.92	0.3	0.07	0.07	90
3	1.97	0.45	0.14	0.14	180
4	2.02	0.6	0.21	0.21	270

The mean value of an index at level i (k_i, i = 1, 2, 3, 4) and the difference between the maximum and minimum values of k_i of a factor (R) are the two key parameters in the range analysis of the orthogonal method. The former helps to determine the optimal level and the latter helps to evaluate the importance of the factors. As each level of a factor occurs in four structures in Table 2, k_i and R can be expressed as

https://doi.org/10.1021/acs.iecr.2c02054
Ind. Eng. Chem. Res. 2022, 61, 14927−14939

Table 2. Orthogonal Table of the Double-Eccentric Design

	factor				
design	D_{ei}/m	h_{ec}/m	L_x/m	L_y/m	θ/°
D01	1.87	0.15	0	0	0
D02	1.87	0.3	0.07	0.07	90
D03	1.87	0.45	0.14	0.14	180
D04	1.87	0.6	0.21	0.21	270
D05	1.92	0.15	0.07	0.14	270
D06	1.92	0.3	0	0.21	180
D07	1.92	0.45	0.21	0	90
D08	1.92	0.6	0.14	0.07	0
D09	1.97	0.15	0.14	0.21	90
D10	1.97	0.3	0.21	0.14	0
D11	1.97	0.45	0	0.07	270
D12	1.97	0.6	0.07	0	180
D13	2.02	0.15	0.21	0.07	180
D14	2.02	0.3	0.14	0	270
D15	2.02	0.45	0.07	0.21	0
D16	2.02	0.6	0	0.14	90

$$k_i = \frac{1}{4}\sum_{j=1}^{4} Y_{ij} \tag{1}$$

$$R = \max_{i=1,2,3,4}\{k_i\} - \min_{i=1,2,3,4}\{k_i\} \tag{2}$$

where Y_i represents the index of the cyclone performance at level i.

3. NUMERICAL APPROACHES

3.1. Mathematical Models. In the current study, the gas is assumed to be incompressible and isothermal inside the cyclone separator. Therefore, the continuity and momentum equations can be written as

$$\frac{\partial \overline{u_i}}{\partial x_i} = 0 \tag{3}$$

$$\rho\frac{\partial \overline{u_i}}{\partial t} + \rho\overline{u_j}\frac{\partial \overline{u_i}}{\partial x_j} = -\frac{\partial \overline{P}}{\partial x_i} + \mu\frac{\partial^2 \overline{u_i}}{\partial {x_j}^2} - \rho\frac{\partial \overline{u_i' u_j'}}{\partial x_j} \tag{4}$$

where t is the time, P is the pressure, μ and ρ are the gas dynamic viscosity and density, respectively, u and u' are the instantaneous velocity and fluctuating velocity, respectively, and x is the position in the Cartesian coordinates.

The Reynolds stress model (RSM) is adopted to model the turbulence and the transport equation of the Reynolds stresses is given as

$$\rho\frac{\partial \overline{u_i' u_j'}}{\partial t} + \rho\frac{\partial u_k\overline{u_i' u_j'}}{\partial x_k} = D_{ij} + P_{ij} + \Pi_{ij} + \varepsilon_{ij} \tag{5}$$

The terms D_{ij}, P_{ij}, Π_{ij}, and ε_{ij} on the right side of eq 5 represent the stress diffusion, shear production, pressure strain, and dissipation, respectively, which are expressed as

$$D_{ij} = -\frac{\partial}{\partial x_k}\left[\rho\overline{u_i' u_j' u_k'} + \overline{p' u_j'}\delta_{ik} + \overline{p' u_i'}\delta_{jk} - \mu\frac{\partial \overline{u_i' u_j'}}{\partial x_k}\right] \tag{6}$$

$$P_{ij} = -\rho\left[\overline{u_i' u_k'}\frac{\partial u_j}{\partial x_k} + \overline{u_j' u_k'}\frac{\partial u_i}{\partial x_k}\right] \tag{7}$$

$$\Pi_{ij} = \overline{p'\left(\frac{\partial u_i'}{\partial x_j} + \frac{\partial u_j'}{\partial x_i}\right)} \tag{8}$$

$$\varepsilon_{ij} = -2\mu\overline{\frac{\partial u_i'}{\partial x_k}\frac{\partial u_j'}{\partial x_k}} \tag{9}$$

The solid particles inside the cyclone are treated using the Lagrangian approach with the discrete phase model (DPM), namely, the particles are treated as the discrete phase and the particle motion is governed by the drag force and gravity. According to the force balance, the trajectory of a particle can be predicted using the following equations

$$\frac{dx_{pi}}{dt} = u_{pi} \tag{10}$$

$$\frac{du_{pi}}{dt} = \frac{18\mu}{\rho_p {d_p}^2}\frac{C_D Re_p}{24}(u_i - u_{pi}) + \frac{g_i(\rho_p - \rho)}{\rho_p} \tag{11}$$

where the particle Reynolds number (Re_p) is defined as

$$Re_p = \frac{\rho d_p(\vec{u} - \overrightarrow{u_p})}{\mu} \tag{12}$$

For spherical particles, the drag coefficient (C_D) can be expressed as

$$C_D = a_1 + \frac{a_2}{Re_p} + \frac{a_3}{{Re_p}^2} \tag{13}$$

where a_1, a_2, and a_3 are constants correlated with Re_p given by Morsi et al.[40]

3.2. Physical Parameters and Boundary Conditions. The numerical simulation aims at the process of removing the particles from the high-temperature flue gas. The density and viscosity of the flue gas at about 900 °C are 0.284 kg/m^3 and 4.86 × 10^{-5} Pa/s^{-1}, respectively. The density of the solid particle is 2400 kg/m^3. The particles with diameters of 20, 30, 40, and 50 μm were selected in the simulation process to evaluate the separation performance of the cyclone.

As for the inlet of the cyclone separator, the gas inlet velocity (u_{in}) is 14.8 m/s and is normal to the boundary. The hydraulic diameter (D_H) and turbulent intensity (I_T) at the inlet are calculated by the following equations[41]

$$D_H = \frac{2a_1 b}{a_1 + b} \tag{14}$$

$$I_T = 0.16\left(\frac{\rho D_H u_{in}}{\mu}\right)^{-0.125} \tag{15}$$

The upper outlet of the vortex finder is of pressure-outlet type with a Gauge pressure of −1500 Pa, which is a common value in a high-temperature fluidized bed system. All of the walls of the simulated cyclone separator are under the nonslip boundary condition. It is noticed here that the bottom outlet of the cone is regarded as the wall for the gas phase.

The solid particles are of the same inlet velocity as the gas flow with 231 particle injection points uniformly set at the inlet. In this study, the diameters of particles injected into the cyclone separator are 20, 30, 40, and 50 μm. The mass flow

https://doi.org/10.1021/acs.iecr.2c02054
Ind. Eng. Chem. Res. 2022, 61, 14927−14939

rates of particles with four different diameters injected by an injection point are the same.

The particles will leave the cyclone separator once they reach one of the two outlets. The particles are regarded as separated particles if they reach the bottom outlet of the cone. While the particles are regarded as the escaped particles if they reach the outlet of the vortex finder. The particles rebound off the walls and both the normal (e_n) and tangent (e_t) restitution coefficients are functions of the impact angle (α)[42]

$$e_n = 1 - 0.0218\alpha + 0.0002\alpha^2 \tag{16}$$

$$e_t = 0.7829 - 0.0041\alpha + 0.00004\alpha^2 \tag{17}$$

3.3. Solution Methods. The mathematical models in this study were solved by Ansys Fluent software. The standard SIMPLE scheme was adopted to couple the pressure and velocity terms. The least squares cell-based and QUICK schemes were used to discretize the gradient and momentum, respectively. The second-order upwind scheme was applied for the spatial discretization of the turbulent kinetic energy and turbulent dissipation rate. The first-order upwind scheme was adopted for the Reynolds stresses discretization. The convergence criteria of 10^{-5} were used for the scaled residual components.

A time step of 0.005 was adopted for the transient numerical simulation of all of the cyclones with various designs for the vortex finder. For each case, 10 000 time steps were carried out, namely, the total flow time was 50 s. The time-average simulated results of the last 1000 time steps, in which the gas flow had already reached stabilization, were used to estimate the flow pattern and performance of the cyclone separator.

As for the solid particles, the discrete random work model was adopted to evaluate the particle dispersion in gas turbulent flow, which has been detailed described by Parvaz et al.[43] The step length factor of 5 was adopted in the particle tracking process.

3.4. Grid Generation and Independence. The structured grids were utilized for the interior flow zone. Different grids of the conventional cyclone separator shown in Figure 1 were taken as an example to test the grid independence. The simulated pressure drop (ΔP) and the facet maximum ($P_{in,max}$) and minimum ($P_{in,min}$) static pressures of the inlet under different cell numbers (ranging from 299 776 to 2 325 135) are shown in Figure 3. To assure the grid independence and also save the calculation time, the generating method with 995 568 cells (see Figure 4) was adopted in the numerical simulation.

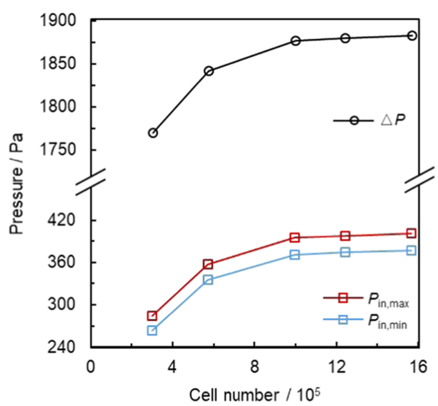

Figure 3. Simulated results for grid independence.

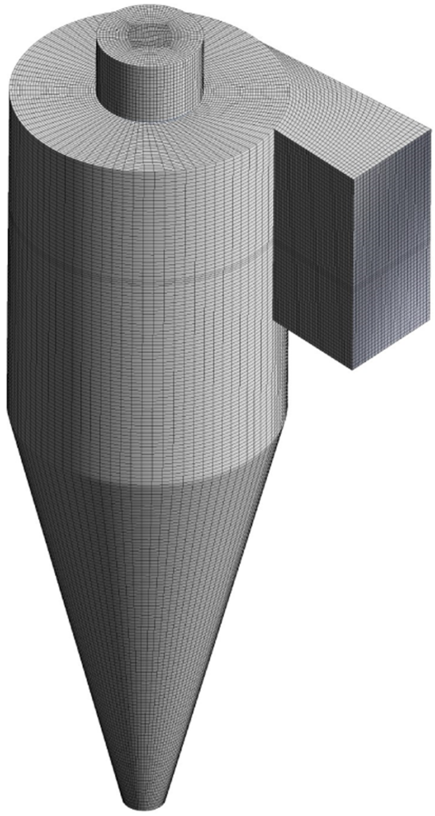

Figure 4. Gird with 995568 cells for the conventional cyclone.

3.5. Validation of the Numerical Approaches. The validation of the numerical approaches has already been conducted in our previous study,[44] where the experimental data reported by Chu et al.[45] and Wang et al.[46] were used to validate the same numerical approaches; see Figure 5a,b. Considering the gas phase in this study is high-temperature flue gas, the simulated results under different gas temperatures were compared with the experimental data reported by Bohnet;[47] see Figure 5c. Although the cyclone separators used in refs 45−47 are of very different structures and working conditions, it can be seen in Figure 5 that the simulated results are always well fitted to the experimental data. The above results are enough to prove that the numerical approaches can simulate the flow pattern and evaluate the performance of a cyclone separator with reasonable accuracy.

In addition, Hoekstra et al.[48] used three turbulence models to simulate the flow pattern inside a cyclone separator and discovered that RSM provided the most accurate results for the strong swirling flow. Since then, RSM and DPM have been widely applied and validated in the numerical studies of different cyclones and working conditions,[5,7,10,15,18,19] which means the numerical approaches in this study are not confined to a specific cyclone separator but are applicable to cyclones of various structures working conditions.

4. RESULTS AND DISCUSSION

4.1. Cyclone Performance and Optimal Structure. The simulated pressure drop of the conventional cyclone separator (ΔP_0) is 1877.09 Pa. The simulated grade separation efficiencies of particles with diameters of 20 μm ($\eta_{0,20}$), 30 μm ($\eta_{0,30}$), 40 μm ($\eta_{0,40}$), and 50 μm ($\eta_{0,50}$) are 38.37, 53.96, 68.02, and 82.77%, respectively. Based on the above simulated

https://doi.org/10.1021/acs.iecr.2c02054
Ind. Eng. Chem. Res. 2022, 61, 14927−14939

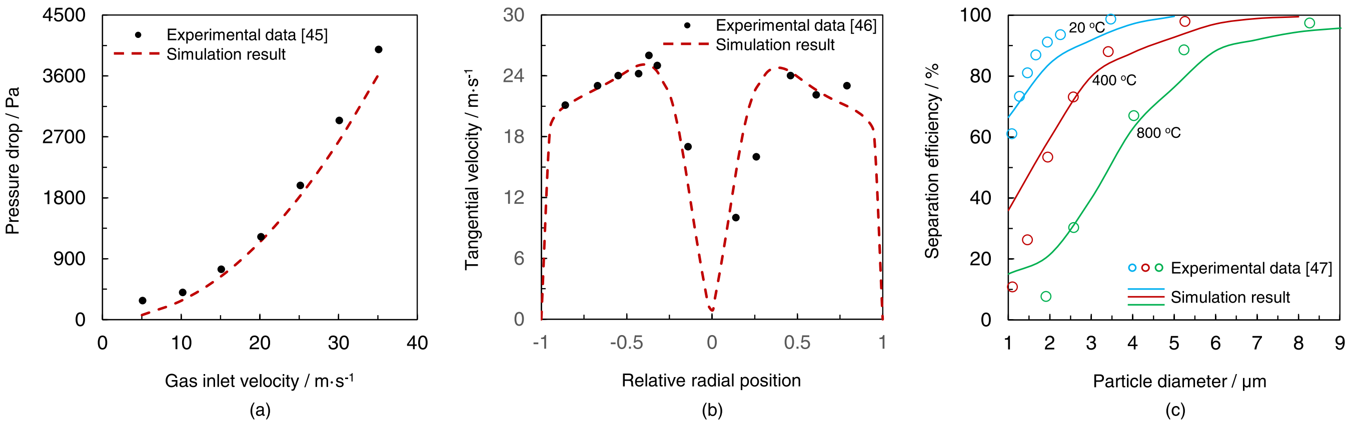

Figure 5. Validation of the numerical approaches.[44] (Permission was obtained from Elsevier).

results, the changes of the cyclone performance including pressure drop ($\Delta P^* = \Delta P - \Delta P_0$) and the grade separation efficiency ($\eta_d^* = \eta_d - \eta_{0,d}$, d = 20, 30, 40, 50) due to the double-eccentric designs for the vortex finder in Table 2 can be estimated and are summarized in Table 3.

Table 3. Changes in Cyclone Performance due to the Double-Eccentric Designs

design	ΔP^*/Pa	η_{20}^*/%	η_{30}^*/%	η_{40}^*/%	η_{50}^*/%
D01	346.89	1.46	2.72	3.77	2.65
D02	280.09	−0.61	0.25	0.41	0.80
D03	249.99	−0.18	−0.24	2.75	3.79
D04	244.02	0.08	1.21	4.44	6.15
D05	126.00	−1.87	−2.37	−1.58	−1.17
D06	−37.65	−4.62	−4.95	−4.98	−5.77
D07	310.73	4.99	7.75	10.54	7.88
D08	209.88	0.21	2.44	5.58	5.13
D09	18.90	−3.92	−5.43	−5.00	−4.71
D10	99.87	−1.88	−2.76	−0.48	0.44
D11	75.75	1.56	0.41	1.54	2.23
D12	179.22	3.70	4.96	7.93	5.94
D13	86.90	−0.25	0.00	1.81	2.06
D14	146.05	3.61	3.40	6.53	5.41
D15	−76.59	−3.45	−4.48	−6.66	−7.91
D16	−64.28	−3.20	−4.23	−5.04	−7.32

The range analysis was carried out to analyze the effects of each factor on the cyclone performance. The range analysis data of ΔP^* and η_d^* are illustrated in Figures 6 and 7, respectively. It can be observed that D_{ei}, L_x, and L_y have powerful effects on ΔP^*. Expanding the inlet of the vortex finder markedly reduces ΔP^*. A larger L_x can also result in a lower ΔP^*, while the effects of h_{ec} and θ on ΔP^* are not significant compared to the other three factors. As shown in Figure 7, L_y always plays the most important role among the five factors in the separation performance, and increasing L_y can effectively enhance the separation performance. Normally, η_d^* can also be improved by decreasing D_{ei}, increasing h_{ec}, and L_x. The results also indicate that θ = 270° is best for particle separation. For all of these five factors, their effects on η_{40}^* and η_{50}^* are greater than those on η_{20}^* and η_{30}^*.

To find out the optimal structure of the double-eccentric vortex finder, ΔP and η_d are normalized using the following equations

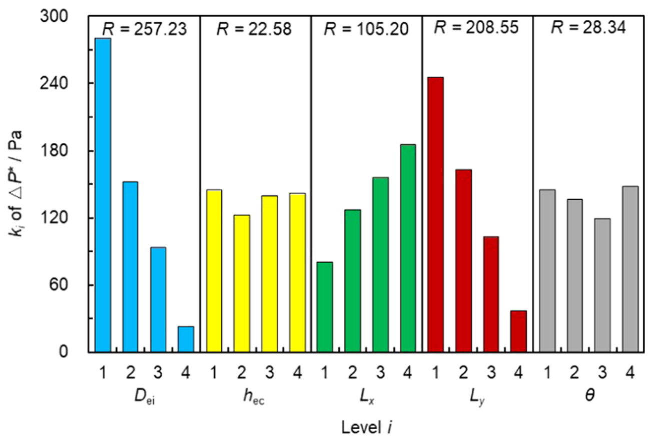

Figure 6. Range analysis data of ΔP^*.

$$\Delta P^{(n)} = \frac{\max\{\Delta P^*\} - \Delta P^*}{\max\{\Delta P^*\} - \min\{\Delta P^*\}} \tag{18}$$

$$\eta_d^{(n)} = \frac{\eta_d^* - \min\{\eta_d^*\}}{\max\{\eta_d^*\} - \min\{\eta_d^*\}} \tag{19}$$

where $\Delta P^{(n)}$ and $\eta_d^{(n)}$ range from 0 to 1.

For a cyclone separator, a larger $\Delta P^{(n)}$ signifies a lower ΔP and a better energy-saving performance. Moreover, a larger $\eta_d^{(n)}$ signifies a better separation performance. Taking both pressure drop and separation efficiency into consideration, the overall performance index of the cyclone (I_ω) is defined as

$$I_\omega = \omega \Delta P^{(n)} + \frac{1-\omega}{4} \sum_{d=20,30,40,50} \eta_d^{(n)} \tag{20}$$

where ω denotes the weighting factor of $\Delta P^{(n)}$ which ranges from 0 to 1. As reported by Ye et al.,[49] the optimal structure of the cyclone separator changes with ω. Considering that the optimization of the vortex finder is primarily for the improvement of the separation efficiency, ω is set to be 0.2 here to evaluate the cyclone performance and also the optimal structure of the double-eccentric vortex finder.

The values of $\Delta P^{(n)}$ and $\eta_d^{(n)}$ are summarized in Table S2 and the values of $I_{0.2}$ are summarized in Table S3 in the Supporting Information. The range analysis data of $I_{0.2}$ are presented in Figure 8. It can be observed that the highest k_i of I for each factor can be distinguished and the best levels of D_{ei}, h_{ec} L_x, L_y, and θ are 2, 4, 4, 1, and 4, respectively. Therefore, the optimal

https://doi.org/10.1021/acs.iecr.2c02054
Ind. Eng. Chem. Res. 2022, 61, 14927−14939

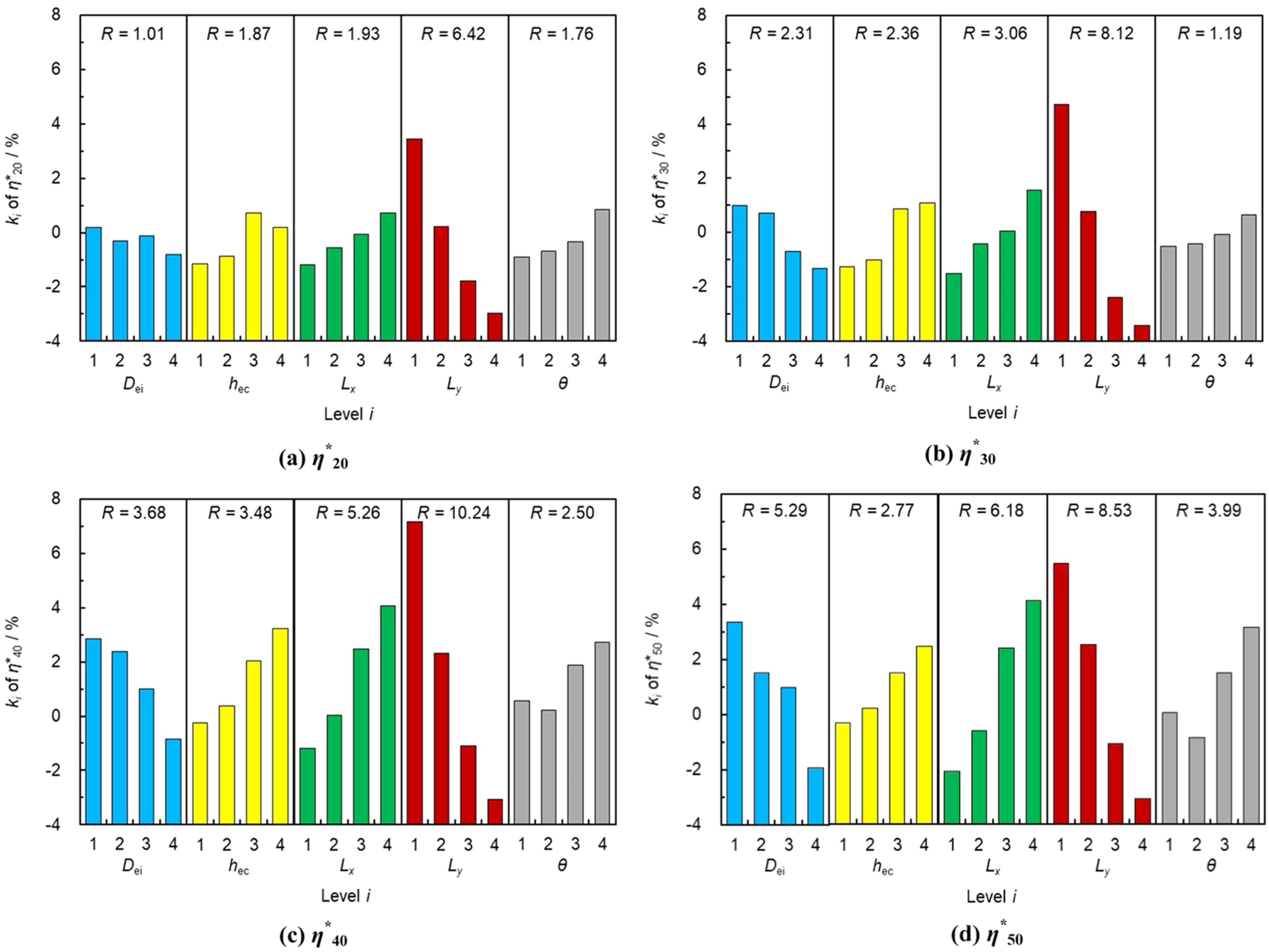

Figure 7. Range analysis data of η^*_d (d = 20, 30, 40, 50).

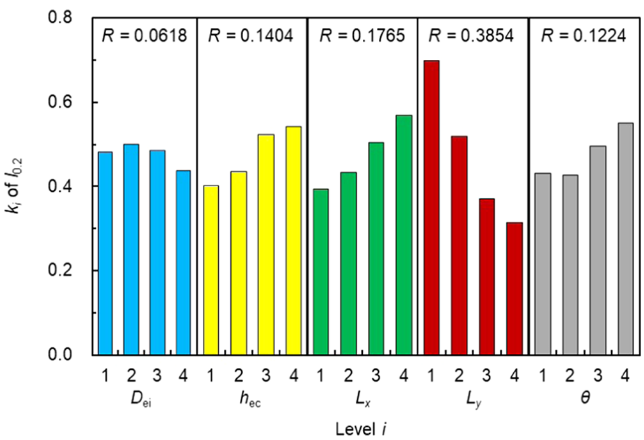

Figure 8. Range analysis data of $I_{0.2}$.

structure of the double-eccentric vortex finder are D_{ei} = 1.92 m, h_{ec} = 0.6 m, L_x = 0.21 m, L_y = 0, and θ = 270°. By comparing R values in Figure 8, the significance of the five factors on the overall cyclone performance can be sorted from the largest to the smallest: $L_y > L_x > h_{ec} > \theta > D_{ei}$. The values of $I_{0.16}$ and $I_{0.24}$ are also listed in Table S3, and the range analysis data of $I_{0.16}$ and $I_{0.24}$ are shown in Figure S1 in the Supporting Information. When ω = 0.16 and 0.24, the best levels and ranking of R values for all of the five parameters are the same as those of ω = 0.2. That indicates the optimal structure keeps unchanged with ω when ω is near 0.2.

Based on the above optimal structure, the performance of cyclones with vortex finders of the original, non-eccentric, single-eccentric, and double-eccentric designs were estimated. The values of the five geometric factors of the four designs and the simulated results of the cyclone performance are listed in Table 4. Compared to the single-eccentric design, the double-eccentric design effectively improves the separation performance and increases ΔP only by less than 50 Pa, which also

Table 4. Geometric Factors and Cyclone Performance of Different Designs for the Vortex Finder

design		original	non-eccentric	single-eccentric	double-eccentric
geometric factor	D_{ei}/m	2.07	1.92	1.92	1.92
	h_{ec}/m	0	0.6	0.6	0.6
	L_x/m	0	0	0.21	0.21
	L_y/m	0	0	0	0
	θ/°				270
cyclone performance	ΔP^*/Pa	0	230.2	329.71	379.59
	η^*_{20}/%	0	4.39	8.02	8.4
	η^*_{30}/%	0	7.08	12.05	14.48
	η^*_{40}/%	0	8.07	14.61	16.86
	η^*_{50}/%	0	6.29	10.03	10.89

https://doi.org/10.1021/acs.iecr.2c02054
Ind. Eng. Chem. Res. 2022, 61, 14927−14939

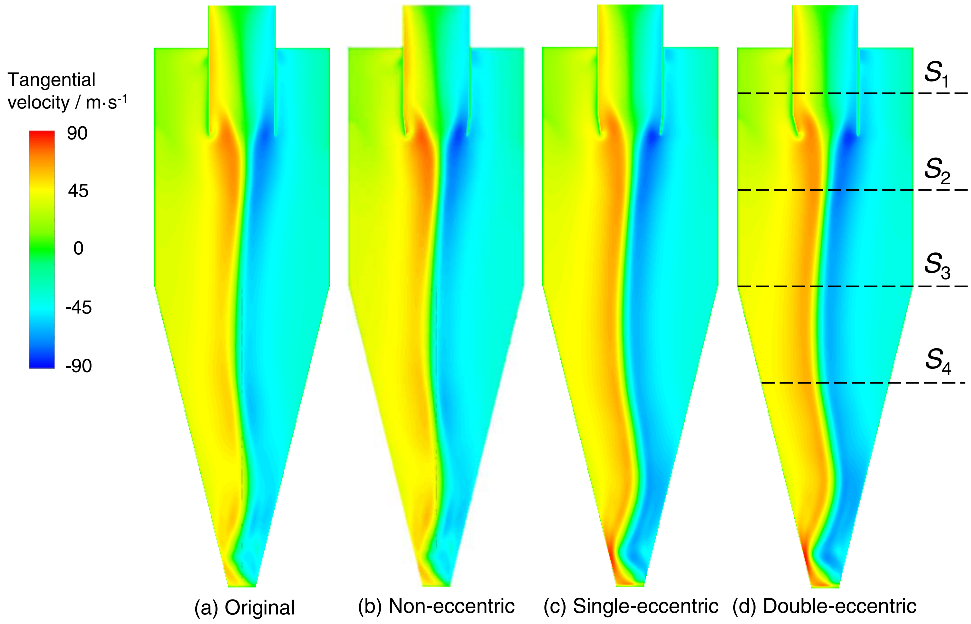

Figure 9. Contour plots of gas tangential velocity.

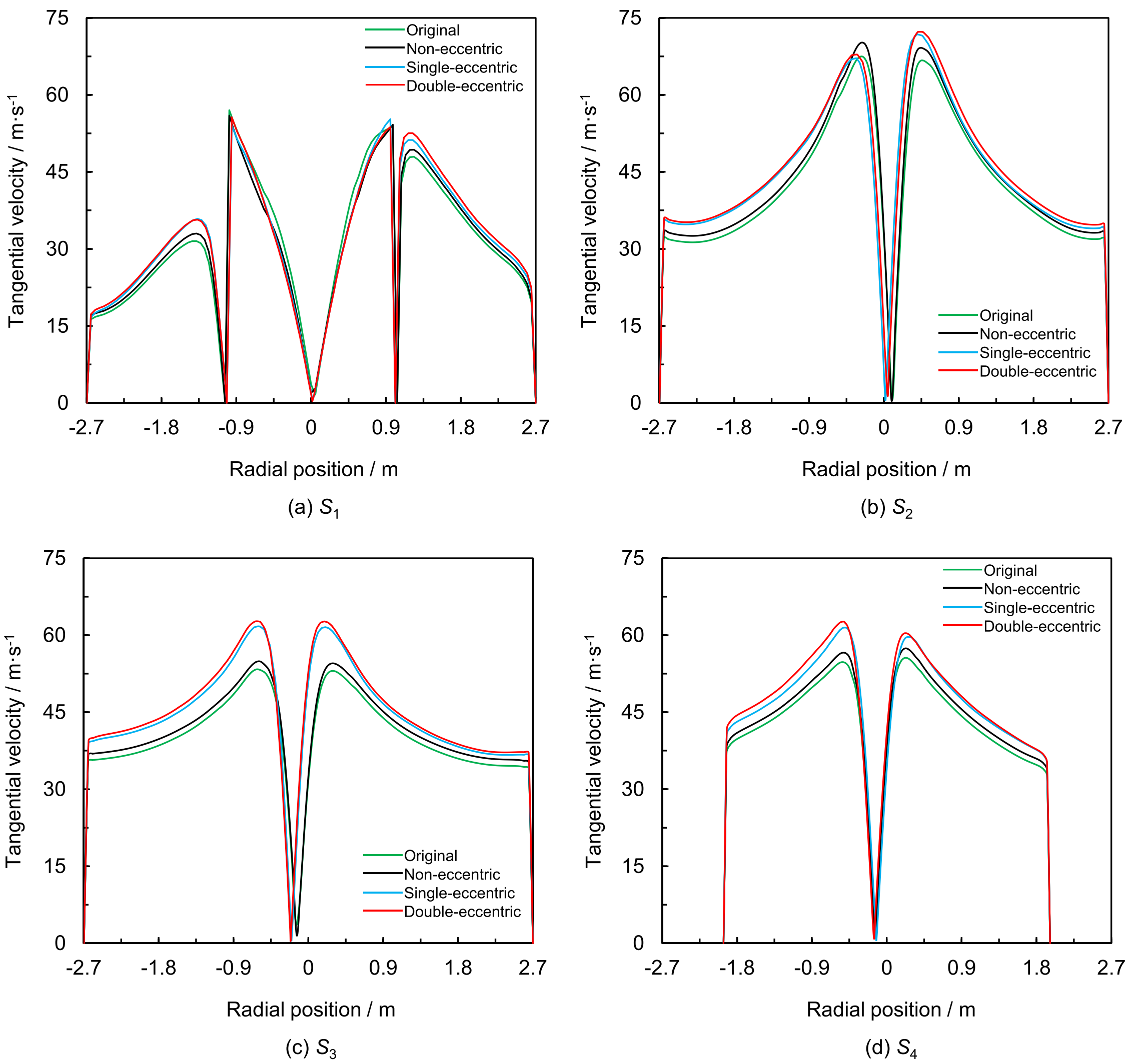

Figure 10. Gas tangential velocity (absolute value) profiles.

https://doi.org/10.1021/acs.iecr.2c02054
Ind. Eng. Chem. Res. 2022, 61, 14927−14939

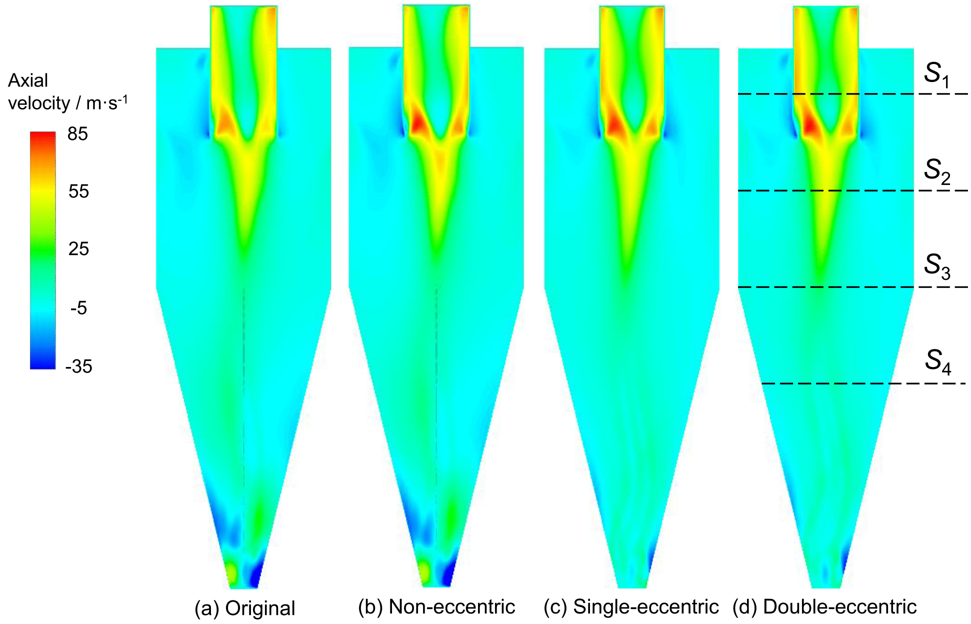

Figure 11. Contour plots of gas axial velocity.

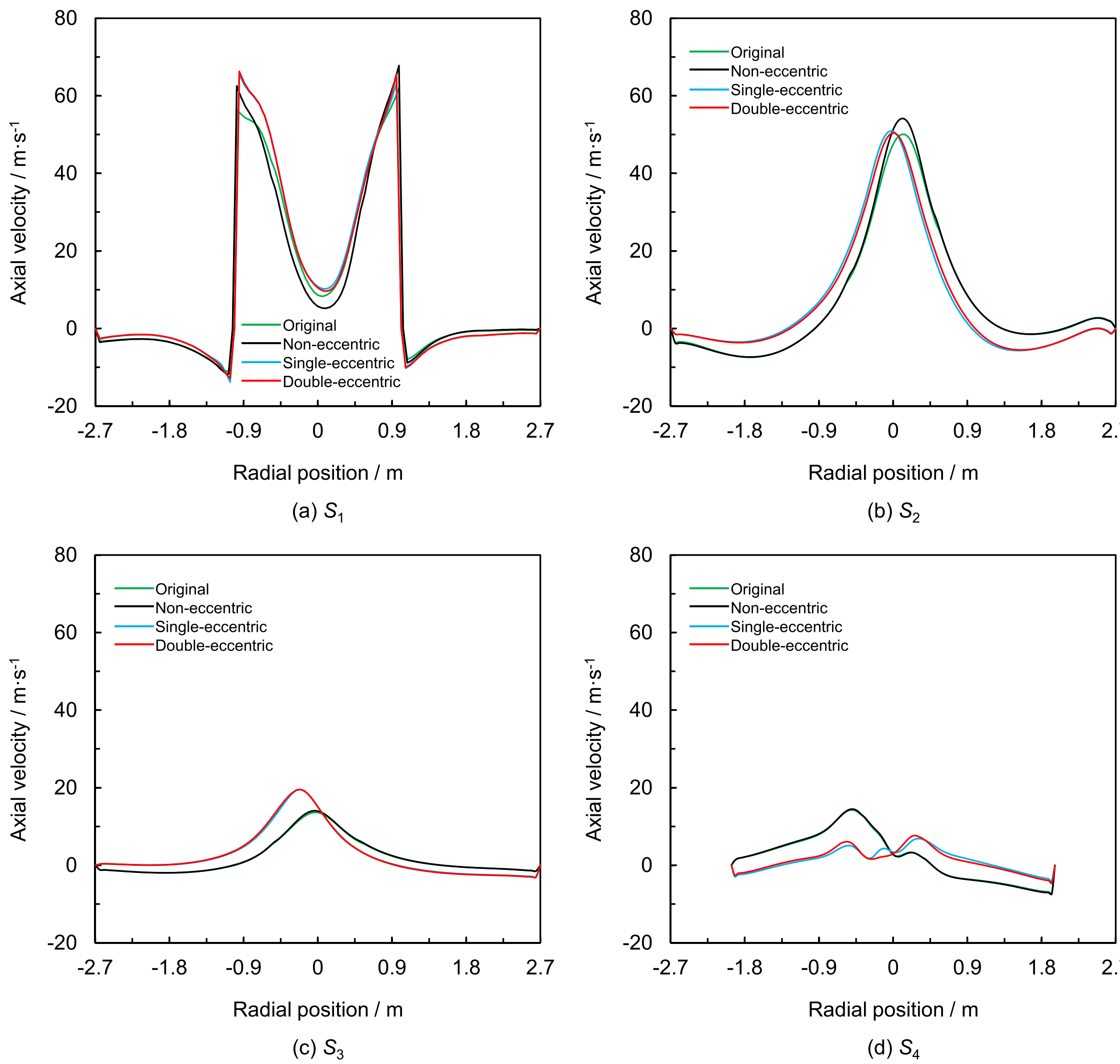

Figure 12. Gas axial velocity profiles.

https://doi.org/10.1021/acs.iecr.2c02054
Ind. Eng. Chem. Res. 2022, 61, 14927−14939

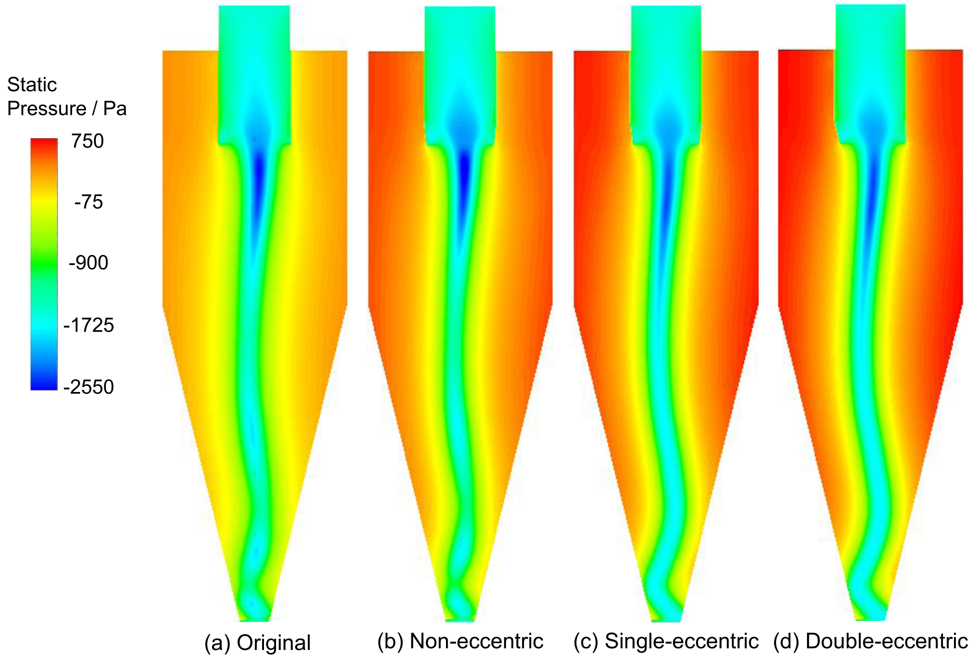

Figure 13. Contour plots of static pressure.

proves that off-centering the inlet of the vortex finder is of benefit to a cyclone separator.

4.2. Flow Patterns. The flow patterns of the cyclones adopting different vortex finder designs in Table 4 were compared for a better understanding of the difference in the cyclone performance.

The contour plots of the gas tangential velocity on the vertical cross section of $x = 0$ in Figure 2 are shown in Figure 9. It can be observed that the distribution of the tangential velocity in the flow zone is similar to the Rankine vortex. In the inner region, the gas tangential velocity increases along the radial direction which forms a quasi-forced vortex. After reaching the peak value, the gas tangential velocity decreases along the radial direction, forming a quasi-free vortex in the outer region.

Four typical horizontal cross sections (S_1−S_4) are marked in Figure 9d and the gas tangential velocity (absolute value) profiles on these sections are shown in Figure 10. It can be observed that the tangential velocities of the single-eccentric and double-eccentric vortex finders are obviously higher than the origin and non-eccentric vortex finders at most positions in the quasi-free vortex region. Based on the single-eccentric vortex finder, off-centering the inlet of the vortex finder causes a small increase in the tangential velocity in the outer region of the cylinder body. The maximum value of the gas tangential velocity in the cylinder body always occurs in the double-eccentric design, indicating that the double-eccentric design results in the strongest swirling flow in the cylinder bodies of the cyclones among the four designs. However, the difference in the tangential velocity between the double-eccentric and single-eccentric vortex finders is far smaller than that between the single-eccentric and non-eccentric vortex finders. This phenomenon reveals that off-centering the vortex finder is the most effective way to increase the gas tangential velocity, enhance the swirling flow, and improve the separation efficiency. Also, L_x and L_y are of more significance than the other three factors in the cyclone performance, which agrees with the results in Figure 8.

The contour plots of the axial tangential velocity on the same vertical cross section are shown in Figure 11. The gas axial velocity profiles on S_1−S_4 are shown in Figure 12. The upper part of the counter plots can also be divided into two regions. An upward flow is located in the inner region, which is surrounded by a downward flow in the outer region. However, this two-region distribution of the axial velocity disappears in the lower part of the cyclone separator where the axial velocity becomes much smaller. As depicted in Figure 12b,c, off-centering the vortex finder makes the peak value of the axial velocity occur in a negative radial position, and consequently increases the downward flow region area in the right part of the counter; see Figure 11c,d. Therefore, off-centering the inlet of the vortex finder to the right side of the counter can decrease the probability of the particle entering the vortex finder with the upward flow.

Figure 13 presents the contour plots of the static pressure. The static pressure increases along the radial direction from the core to the wall due to the strong swirling flow. From the original design to the double-eccentric design, the low-pressure region in the center of the cyclone separator becomes broader and twister.

Moreover, the pressure drops between the bottom of the cylinder entrance and the bottom of the vortex finder wall of the original, non-eccentric, single-eccentric, and double-eccentric designs are 637.9, 764.2, 630.5, and 648.3 Pa, respectively. As reported by Cocco et al.,[35] this pressure drop has a positive correlation with the intensity of the secondary swirling flow near the vortex finder. Off-centering the vortex finder markedly reduces this kind of pressure drop and weakens the secondary swirling flow. That is also a reason why off-centering the vortex finder is the most effective way to improve the separation efficiency.

4.3. Industrial Test. Most gas−solid fluidized bed systems adopt cyclone separators to collect the particles and maintain the material balance.[50−53] As an indispensable component for the CFB boiler, the cyclone separator plays a major role in the

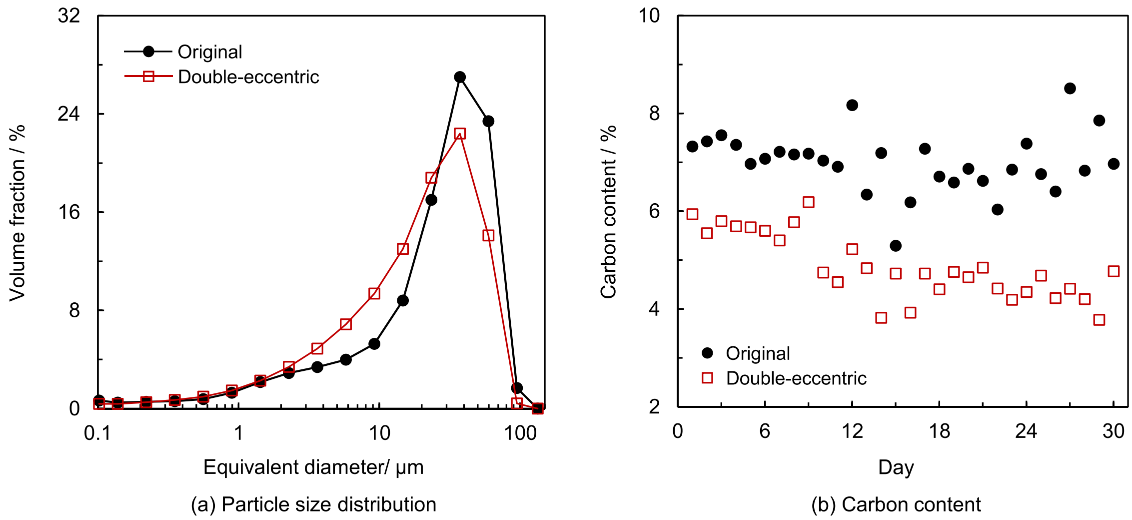

Figure 14. Measured results of the fly ash samples.

stable operation, which is expected with high separation efficiency.

An industrial test of the double-eccentric design was conducted in two same 240 t/h CFB boilers, both of which are equipped with two parallel hot cyclone separators. The wall of the hot cyclone separator is made of the abrasion-resistant refractory, the outer steel layer, and the steel studs. In this test, the cyclone separators were retrofitted with the double-eccentric vortex finders while the vortex finders of the other same CFB boiler in this power plant were still of the original design. For the double-eccentric vortex finders, D_{ei}/D_e, h_{ec}/L_e, L_x/D, L_y/D, and θ are equal to the values of the optimal structure in Table 4 and the basic cyclone structure in Table S1 in the Supporting Information.

Induced fans were used to force the high-temperature flue gas to pass the cyclone separators and the tail. The fly ash in the flue gas was collected by the filters at the end of the tail before the flue gas entering the induced fans. The fly ash samples of the two CFB boilers were taken for 30 consecutive days in which the two boilers kept the same feeding coal and also the same operating condition. The pressure drop of the cyclone separators was also recorded. The average solid load rating at the inlet of each cyclone was about 5.5 kg/kg of flue gas. The particle size and the carbon content of the fly ash samples were measured by laser particle size analysis and proximate analysis, respectively. Some measured results of the fly ash samples are shown in Figure 14. Taking the samples of the first day as an example (see Figure 14a), the double-eccentric vortex finder makes the fly ash finer compared to the original vortex finder, indicating that the double-eccentric vortex finder can successfully enhance the separation performance.

The better separation performance means that the double-eccentric vortex finder causes more particles in the cyclone separator to enter the dipleg rather than the tail and finally move back to the furnace. As a result, the average residence time of the fuel particles in the circulating loop of the CFB boiler is extended and the combustion efficiency of the fuel particles is improved, which can be reflected in Figure 14b. This figure depicts that the fly ash samples of the double-eccentric vortex finder always contain less carbon content than the samples of the original vortex finder in these 30 days, and the double-eccentric vortex finder reduces the average carbon content by more than 30%. This phenomenon reveals that the double-eccentric vortex finder significantly reduces the heat loss due to unburned carbon in fly ash, and therefore improves the operation efficiency of the CFB boiler. In addition, the double-eccentric vortex finders increase the average pressure drops of the two cyclone separators by 30.7 and 99.1 Pa, respectively, which indicates the double-eccentric vortex finder has a very limited impact on the pressure drop.

5. CONCLUSIONS

In this study, a double-eccentric design for the vortex finder was proposed to optimize the cyclone separator. A numerical simulation was conducted to simulate the flow pattern and evaluate the cyclone performance. To obtain the optimal structure of the double-eccentric vortex finder and analyze the effects of each factor on the cyclone performance, the orthogonal method was adopted and the range analysis was carried out.

The inlet diameter of the vortex finder and the eccentricities of the vortex finder in the x and y directions have powerful effects on the pressure drop. The pressure drop of the cyclone separator can be markedly reduced by expanding the inlet of the vortex finder and moving the vortex finder along the x direction. The eccentricity of the vortex finder in the y direction is the most significant factor in the separation performance. The separation efficiency can be improved by moving the vortex finder along the y direction, narrowing the inlet of the vortex finder, and heightening the conical part. According to the overall performance index, the optimal design for the vortex finder was obtained. The inlet diameter of the vortex finder is 1.92 m, the height of the conical part is 0.6 m, and the eccentricities of the vortex finder in the x and y directions are 0.21 m and 0, respectively, the eccentric angle of the inlet of the vortex finder is 270°. Compared to the single-eccentric design, the double-eccentric design effectively improves the separation performance and slightly increases the pressure drop.

Compared with the original, non-eccentric, and single-eccentric designs, the double-eccentric designs cause the highest gas tangential velocity in the middle and lower parts of the cyclone. Off-centering the vortex finder has the most significant impact on the flow pattern, implying the cyclone

https://doi.org/10.1021/acs.iecr.2c02054
Ind. Eng. Chem. Res. 2022, 61, 14927−14939

performance is more sensitive to the eccentricity of the vortex finder, which agrees with the results in the range analysis.

An industrial test was also conducted in two same CFB boilers equipped with two parallel cyclone separators. The fly ash samples of the CFB boiler retrofitted with double-eccentric vortex finders become finer and contain less carbon content than those of the CFB boiler with origin vortex finders. These phenomena can both reflect the improvement of the separation performance as a result of the double-eccentric vortex finder.

■ ASSOCIATED CONTENT

Supporting Information

The Supporting Information is available free of charge at https://pubs.acs.org/doi/10.1021/acs.iecr.2c02054.

Detailed geometric dimensions of the cyclone separator; values of $\Delta P^{(n)}$, $\eta_d^{(n)}$, and I_ω of the cyclone separators with different designs for the vortex finder; and range analysis data of $I_{0.16}$ and $I_{0.24}$ (PDF)

■ AUTHOR INFORMATION

Corresponding Author

Zhong Huang − *Key Laboratory for Thermal Science and Power Engineering of Ministry of Education, Department of Energy and Power Engineering, Tsinghua University, Beijing 100084, China;* orcid.org/0000-0002-3996-1728; Phone: +86-10-62781559; Email: huangzhong@mail.tsinghua.edu.cn

Authors

Yuge Yao − *Key Laboratory for Thermal Science and Power Engineering of Ministry of Education, Department of Energy and Power Engineering, Tsinghua University, Beijing 100084, China;* orcid.org/0000-0002-6420-8519

Tuo Zhou − *Key Laboratory for Thermal Science and Power Engineering of Ministry of Education, Department of Energy and Power Engineering, Tsinghua University, Beijing 100084, China;* orcid.org/0000-0002-9787-1755

Jinjing Li − *North China Electric Power Research Institute, Beijing 100045, China*

Liang Cheng − *North China Electric Power Research Institute, Beijing 100045, China*

Man Zhang − *Key Laboratory for Thermal Science and Power Engineering of Ministry of Education, Department of Energy and Power Engineering, Tsinghua University, Beijing 100084, China*

Hairui Yang − *Key Laboratory for Thermal Science and Power Engineering of Ministry of Education, Department of Energy and Power Engineering, Tsinghua University, Beijing 100084, China;* orcid.org/0000-0002-0625-7320

Junfu Lyu − *Key Laboratory for Thermal Science and Power Engineering of Ministry of Education, Department of Energy and Power Engineering, Tsinghua University, Beijing 100084, China;* orcid.org/0000-0002-8258-3662

Complete contact information is available at: https://pubs.acs.org/10.1021/acs.iecr.2c02054

Notes

The authors declare no competing financial interest.

■ ACKNOWLEDGMENTS

This research was supported by the State Grid Jibei Electric Power Company Science and Technology Project (SGTYHT/21-JS-225) and the Huaneng Group Science and Technology Research Project (HNKJ21-H31).

■ REFERENCES

(1) Zhang, T.; Liu, C.; Guo, K.; Liu, H.; Wang, Z. Analysis of Flow Field in Optimal Cyclone Separators with Hexagonal Structure Using Mathematical Models and Computational Fluid Dynamics Simulation. *Ind. Eng. Chem. Res.* **2016**, *55*, 351−365.

(2) Wang, B.; Li, S. Q.; Dong, S. J.; Xin, R. B.; Jin, R. Z.; Zhang, Y. M.; Dong, K. J.; Jiang, Y. C. A New Fine Particle Removal Technology: Cloud-Air-Purifying. *Ind. Eng. Chem. Res.* **2018**, *57*, 11815−11825.

(3) Iozia, D. L.; Leith, D. Effect of Cyclone Dimensions on Gas Flow Pattern and Collection Efficiency. *Aerosol Sci. Technol.* **1989**, *10*, 491−500.

(4) Kim, J. C.; Lee, K. W. Experimental Study of Particle Collection by Small Cyclones. *Aerosol Sci. Technol.* **1990**, *12*, 1003−1015.

(5) El-Batsh, H. M. Improving Cyclone Performance by Proper Selection of the Exit Pipe. *Appl. Math. Modell.* **2013**, *37*, 5286−5303.

(6) Elsayed, K.; Lacor, C. The Effect of Cyclone Vortex Finder Dimensions on the Flow Pattern and Performance Using LES. *Comput. Fluids* **2013**, *71*, 224−239.

(7) Zhang, Z.-W.; Li, Q.; Zhang, Y.; Wang, H. Simulation and Experimental Study of Effect of Vortex Finder Structural Parameters on Cyclone Separator Performance. *Sep. Purif. Technol.* **2022**, *286*, No. 120394.

(8) Razmi, H.; Goharrizi, A. S.; Mohebbi, A. CFD Simulation of an Industrial Hydrocyclone Based on Multiphase Particle in Cell (MPPIC) Method. *Sep. Purif. Technol.* **2019**, *209*, 851−862.

(9) Hwang, I. S.; Jeong, H. J.; Hwang, J. Effects of Vortex Finder Length on Flow Field and Collection Efficiency of Cyclone in an Industrial-Scale Circulating Fluidized Bed Boiler: Numerical Study. *Int. J. Energy Res.* **2020**, *44*, 7229−7241.

(10) Tian, J.; Ni, L.; Song, T.; Zhao, J. CFD Simulation of Hydrocyclone-Separation Performance Influenced by Reflux Device and Different Vortex-Finder Lengths. *Sep. Purif. Technol.* **2020**, *233*, No. 116013.

(11) Lim, K. S.; Kim, H. S.; Lee, K. W. Characteristics of the Collection Efficiency for a Cyclone with Different Vortex Finder Shapes. *Aerosol Sci. Technol.* **2004**, *35*, 743−754.

(12) Ghodrat, M.; Kuang, S. B.; Yu, A. B.; Vince, A.; Barnett, G. D.; Barnett, P. J. Numerical Analysis of Hydrocyclones with Different Vortex Finder Configuration. *Miner. Eng.* **2014**, *63*, 125−138.

(13) Wang, Z.; Sun, G.; Jiao, Y. Experimental Study of Large-Scale Single and Double Inlet Cyclone Separators with Two Types of Vortex Finder. *Chem. Eng. Process.* **2020**, *158*, No. 108188.

(14) Elsayed, K. Design of a Novel Gas Cyclone Vortex Finder Using the Adjoint Method. *Sep. Purif. Technol.* **2015**, *142*, 274−286.

(15) Misiulia, D.; Antonyuk, S.; Andersson, A. G.; Lundström, T. S. High-Efficiency Industrial Cyclone Separator: A CFD Study. *Powder Technol.* **2020**, *364*, 943−953.

(16) De Souza, F. J.; Salvo, R. V.; Martins, D. M. Effects of the Gas Outlet Duct Length and Shape on the Performance of Cyclone Separators. *Sep. Purif. Technol.* **2015**, *142*, 90−100.

(17) Luo, G.; Cheng, L.; Li, L.; Wang, J.; Jiang, X.; Zhang, W. Effect of Connection Resistance Between Cyclones and Backpass on Furnace Solids Suspension Density Profile and Circulation Rates in CFB. *Energies* **2021**, *14*, No. 6162.

(18) Fu, S.; Zhou, F.; Sun, G.; Yuan, H.; Zhu, J. Performance Evaluation of Industrial Large-Scale Cyclone Separator with Novel Vortex Finder. *Adv. Powder Technol.* **2021**, *32*, 931−939.

(19) Pei, B.; Yang, L.; Dong, K.; Jiang, Y.; Du, X.; Wang, B. The Effect of Cross-Shaped Vortex Finder on the Performance of Cyclone Separator. *Powder Technol.* **2017**, *313*, 135−144.

(20) Dziubak, T. Experimental Research on Separation Efficiency of Aerosol Particles in Vortex Tube Separators with Electric Field. *Bull. Pol. Acad. Sci.* **2020**, *68*, 503−516.

(21) Zhao, Q.; Cui, B.; Wei, D.; Song, T.; Feng, Y. Numerical Analysis of the Flow Field and Separation Performance in Hydro-

https://doi.org/10.1021/acs.iecr.2c02054
Ind. Eng. Chem. Res. 2022, 61, 14927−14939

cyclones with Different Vortex Finder Wall Thickness. *Powder Technol.* **2019**, *345*, 478−491.
(22) Vakamalla, T. R.; Koruprolu, V. B. R.; Arugonda, R.; Mangadoddy, N. Development of Novel Hydrocyclone Designs for Improved Fines Classification. *Sep. Purif. Technol.* **2017**, *175*, 481−497.
(23) Wakizono, Y.; Maeda, T.; Fukui, K.; Yoshida, H. Effect of Ring Shape Attached on Upper Outlet Pipe on Fine Particle Classification of Gas-Cyclone. *Sep. Purif. Technol.* **2015**, *141*, 84−93.
(24) Qiang, L.; Wang, Q.; Xu, W.; Zhu, Z.; Zhu, K. Experimental and Computational Analysis of a Cyclone Separator with a Novel Vortex Finder. *Powder Technol.* **2020**, *360*, 398−410.
(25) Dziubak, T. Experimental Investigation of Possibilities to Improve Filtration Efficiency of Tangential Inlet Return Cyclones by Modification of Their Design. *Energies* **2022**, *15*, 3871.
(26) Chen, J.; Lu, X.; Liu, H.; Yang, C. Effect of the Bottom-Contracted and Edge-Sloped Vent-Pipe on the Cyclone Separator Performance. *Chem. Eng. J.* **2007**, *129*, 85−90.
(27) Chang, M.; Lu, D.; Gao, S.; Fan, Y.; Lu, C. Effects of the Swirl Space Ratio on the Performance of a Coupling Cyclone with a Built-In Granular Bed Filter: An Experimental Examination. *Ind. Eng. Chem. Res.* **2021**, *60*, 571−582.
(28) Muschelknautz, U.; Muschelknautz, E. Separation Efficiency of Recirculating Cyclones in Circulating Fluidized Bed Combustions. *VGB PowerTech* **1999**, *79*, 48−53.
(29) Su, J.; Zhao, X.; Zhang, J.; Liu, A.; Yang, H.; Yue, G.; Fu, Z. In *Design and Operation of CFB Boilers with Low Bed Inventory*, *Proceedings of the 20th International Conference on Fluidized Bed Combustion*; Yue, G.; Zhang, H.; Zhao, C.; Luo, Z., Eds.; Springer: Berlin, Heidelberg, 2012; pp 212−218.
(30) Lalak, I.; Seeber, J.; Kluger, F.; Krupka, S. In *Operational Experience with High Efficiency Cyclones: Comparison Between Boiler A and B in the Zeran Power Plant -- Warsaw, Poland*, *Proceedings of 17th International Conference on Fluidized Bed Combustion*; Pisupati, S. V., Ed.; American Society of Mechanical Engineers (ASME): New York, 2003; pp 685−690.
(31) Yue, G.; Cai, R.; Lu, J.; Zhang, H. From a CFB Reactor to a CFB Boiler - The Review of R&D Progress of CFB Coal Combustion Technology in China. *Powder Technol.* **2017**, *316*, 18−28.
(32) Mirek, P. Influence of the Model Scale on Hydrodynamic Scaling in CFB Boilers. *Braz. J. Chem. Eng.* **2016**, *33*, 885−896.
(33) Brar, L. S.; Elsayed, K. Analysis and Optimization of Cyclone Separators with Eccentric Vortex Finders Using Large Eddy Simulation and Artificial Neural Network. *Sep. Purif. Technol.* **2018**, *207*, 269−283.
(34) Parvaz, F.; Hosseini, S. H.; Ahmadi, G.; Elsayed, K. Impacts of the Vortex Finder Eccentricity on the Flow Pattern and Performance of a Gas Cyclone. *Sep. Purif. Technol.* **2017**, *187*, 1−13.
(35) Cocco, R. A.; Muschelknautz, U.; Freireich, B.; Karri, S. B. R.; Knowlton, T. In *Attributes of an Eccentrically Positioned Vortex Finder on Primary Cyclones*, *Proceedings of 13th International Conference on Fluidized Bed Technology*; Bi, X.; Briens, C.; Ellis, N.; Wormsbecker, M., Eds.; GLAB Reactor and Fluidization Technologies: Vancouver, 2021; pp 593−598.
(36) Mirek, P. The Impact of Scaling Rules on Parameters of the Cyclone Working with CFB Boilers. *Fuel Process. Technol.* **2018**, *169*, 71−76.
(37) Wu, X.; Leung, D.Y.C. Optimization of Biodiesel Production from Camelina Oil Using Orthogonal Experiment. *Appl. Energy* **2011**, *88*, 3615−3624.
(38) Gao, P.; Xu, S. J.; Xu, Z. L.; Li, P.; Wu, Y. Z.; Li, L. Q.; Zhang, H. Z. High-Flux Fine Hollow Fiber Nanofiltration Membranes for the Purification of Drinking Water. *Ind. Eng. Chem. Res.* **2021**, *60*, 1817−1828.
(39) Yang, M.; Zhang, Y.; Wang, Q.; Zhu, Y.; Taylor, R. A. A Coupled Structural-Optical Analysis of a Novel Umbrella Heliostat. *Sol. Energy* **2022**, *231*, 880−888.
(40) Morsi, S. A.; Alexander, A. J. An Investigation of Particle Trajectories in Two-Phase Flow Systems. *J. Fluid Mech.* **1972**, *55*, 193−208.
(41) Wei, Q.; Sun, G.; Gao, C. Numerical Analysis of Axial Gas Flow in Cyclone Separators with Different Vortex Finder Diameters and Inlet Dimensions. *Powder Technol.* **2016**, *295*, 209−217.
(42) Feng, L.; Wang, J.; Wu, Y.; Zhang, H.; Zhang, M.; Lyu, J. Experimental and Numerical Investigation on Effect of Particle Characteristics on Performance of Plate-Type Impact Separator. *CIESC J.* **2018**, *69*, 3348−3355.
(43) Parvaz, F.; Hosseini, S. H.; Elsayed, K.; Ahmadi, G. Influence of the Dipleg Shape on the Performance of Gas Cyclones. *Sep. Purif. Technol.* **2020**, *233*, No. 116000.
(44) Yao, Y.; Huang, W.; Wu, Y.; Zhang, Y.; Zhang, M.; Yang, H.; Lyu, J. Effects of the Inlet Duct Length on the Flow Field and Performance of a Cyclone Separator with a Contracted Inlet Duct. *Powder Technol.* **2021**, *393*, 12−22.
(45) Chu, K. W.; Wang, B.; Xu, D. L.; Chen, Y. X.; Yu, A. B. CFD-DEM Simulation of the Gas−Solid Flow in a Cyclone Separator. *Chem. Eng. Sci.* **2011**, *66*, 834−847.
(46) Wang, B.; Xu, D. L.; Chu, K. W.; Yu, A. B. Numerical Study of Gas-Solid Flow in a Cyclone Separator. *Appl. Math. Modell.* **2006**, *30*, 1326−1342.
(47) Bohnet, M. Influence of the Gas Temperature on the Separation Efficiency of Aerocyclones. *Chem. Eng. Process.* **1995**, *34*, 151−156.
(48) Hoekstra, A. J.; Derksen, J. J.; Van Den Akker, H. E. A. An Experimental and Numerical Study of Turbulent Swirling Flow in Gas Cyclones. *Chem. Eng. Sci.* **1999**, *54*, 2055−2065.
(49) Ye, Q.; Duan, P.; Kuang, S.; Ji, L.; Zou, R.; Yu, A. Multi-Objective Optimization of Hydrocyclone by Combining Mechanistic and Data-Driven Models. *Powder Technol.* **2022**, *407*, No. 117674.
(50) Castilla, G. M.; MontañÉS, R. M.; PallarÈS, D.; Johnsson, F. Dynamic Modeling of the Reactive Side in Large-Scale Fluidized Bed Boilers. *Ind. Eng. Chem. Res.* **2021**, *60*, 3936−3956.
(51) Yao, Y.; Huang, Z.; Zhang, M.; Yang, H.; Lyu, J.; Wang, J. Effects of the Y-Shape Stud and Outer Insulating Layer on Heat Dissipation and Wall Temperature of the Hot Cyclone in a Circulating Fluidized Bed Boiler. *Appl. Therm. Eng.* **2022**, *204*, No. 117989.
(52) Cui, Y.; Zhong, W.; Liu, X.; Xiang, J. Gas-Solid Hydrodynamics and Combustion Characteristics in a 600 MW Annular CFB Boiler for Supercritical CO_2 Cycles. *Ind. Eng. Chem. Res.* **2020**, *59*, 21617−21629.
(53) Qi, G.; Liu, X.; Wang, Z.; Zhang, S.; Guan, J.; Chen, J.; Liu, H. Numerical Simulation and Optimization of Heat-Insulation Material and Structure for CFB Boiler. *Therm. Sci. Eng. Prog.* **2020**, *20*, No. 100692.

https://doi.org/10.1021/acs.iecr.2c02054
Ind. Eng. Chem. Res. 2022, 61, 14927−14939